# Novel Design of a Lowpass-Bandpass Diplexer with an Exceptional Performance Using Microstrip Meandrous Loaded Lines for Microwave Systems

Salah I. Yahya<sup>1</sup>, Mohammed Abdel Hafez<sup>2</sup>, Leila Nouri<sup>3,4†</sup> and Farid Zubir<sup>5</sup>

<sup>1</sup>Department of Computer Technology Engineering, College of Technical Engineering, Al-Hadba University, Mosul, Iraq

<sup>2</sup>Department of Electrical and Communication Engineering, United Arab Emirates University, Al Ain, United Arab Emirates

> <sup>3</sup>Institute of Research and Development, Duy Tan University, Da Nang, Vietnam

> <sup>4</sup>School of Engineering and Technology, Duy Tan University, Da Nang, Vietnam

<sup>5</sup>Wireless Communication Centre, Faculty of Electrical Engineering, Universiti Teknologi Malaysia, Johor Bahru, Johor, Malaysia

Abstract—A new microstrip lowpass-bandpass diplexer with exceptional performance characteristics is designed and analyzed. It includes microstrip meandrous thin lines loaded by solid cells. The diplexer achieves 0.058 dB and 0.013 dB low insertion losses and 26.4% wide fractional bandwidth. Operating frequencies are obtained using a perfect mathematical method, which are verified by the simulation results. Having two equations that accurately predict the operating frequencies allows us to optimize the diplexer's performance by adjusting key parameters such as line lengths and widths. This helps in achieving the desired operating frequencies with minimal trial and error. It has 0.01  $\lambda g^2$  very compact size and exhibits low group delays at both channels, which make it appropriate for a varied range of applications requiring high precision and efficiency. Overall, this microstrip diplexer design offers a versatile and reliable solution for demanding RF and microwave applications.

*Index Terms*—Diplexer, Fractional bandwidth, Insertion loss, Lowpass-bandpass, Microstrip.

# I. Introduction

Microstrip devices are important components in RF and microwave communications. Their application is to separate or combine signals with different frequency channels (Roshani, et al., 2023; Yahya, et al., 2025; Nouri, et al., 2023).

ARO-The Scientific Journal of Koya University Vol. XIII, No.2 (2025), Article ID: ARO.12549. 10 pages DOI: 10.14500/aro.12549

ARO p-ISSN: 2410-9355, e-ISSN: 2307-549X

Received: 24 August 2025; Accepted: 15 November 2025

Regular research paper; Published: 01 December 2025

†Corresponding author's e-mail: Leilanouri@duytan.edu.vn

Copyright © 2025 Salah. I. Yahya, Mohammed Abdel Hafez,

Leila Nouri and Farid Zubir. This is an open-access article distributed under the Creative Commons Attribution License (CC BY-NC-SA 4.0).



The diplexers are designed using microstrip technology, which involves creating transmission lines on a substrate such as a printed circuit board (Jamshidi, et al., 2023; Taghvaei, Bayderkhani and Espahbodi, 2022; Majdi and Mezaal, 2022). The lowpass-bandpass (LP-BP) diplexers consist of two filters - a band-pass filter (BPF) and a lowpass filter (LPF) - combined in a single structure (Rezaei, et al., 2019; Srikanth and Jeyalakshmi 2014). The lowpass filter allows signals below a certain cutoff frequency to pass through, whereas the BPF transmits signals within a chosen frequency range. This enables the diplexer to separate signals based on their frequency content. These diplexers are widely used in various applications, such as radars and wireless networks (Rayatzadeha and Moloudian, 2019; Bavandpour, et al., 2021). They are important in handling signal interference and ensuring efficient signal transmission within different frequency bands. The design and optimization of microstrip LP-BP diplexers require careful consideration of parameters, that is, return and insertion losses (ILs), fractional bandwidth (FBW), group delay (GD), and isolation to meet the specific requirements of the system. Accordingly, several LP-BP diplexers are proposed in (Heshmati and Roshani, 2018; Hayati, et al., 2021; Elden and Gorur, 2021; Hayati, et al., 2019; Nouri, Yahya and Rezaei, 2020; Perez, et al., 2019; Yahya, et al., 2020; Capstick, 1999; Rezaei, Yahya and Nouri, 2023; Deng and Tsai, 2013), utilizing microstrip structures. The first common problem of all LP-BP diplexers (cited in this work) is their huge size. None of them could reduce the size below 0.01λg2. Therefore, introducing a LP-BP diplexer with a size  $<0.01\lambda g2$  and acceptable performance can be a new evolution in design. Having high insertion and return losses in (Hayati, et al., 2021; Elden and Gorur, 2021; Deng and Tsai, 2013; Heshmati and Roshani, 2018; Nouri, Yahya

and Rezaei, 2020; Capstick, 1999), very narrow bandpass channels in (Srikanth and Jeyalakshmi, 2014; Rayatzadeha and Moloudian, 2019; Elden and Gorur, 2021; Deng and Tsai, 2013; Perez, et al., 2019; Yahya, et al., 2021), and harmonics in (Srikanth and Jeyalakshmi, 2014; Bavandpour, et al., 2021; Yahya, et al., 2020; Capstick, 1999; Rezaei, Yahya and Nouri, 2023) are the other problems of previously reported LP-BP diplexers. In (Hayati, et al., 2021) and (Hayati, Rezaei and Noori, 2019), the maximum GD is high, and there is no information about the GDs of the majority of previous LP-BP diplexers.

We want to reach a novel microstrip LP-BP diplexer with the overall dimensions  $0.01\lambda g^2$  and a decent frequency response. Its cutoff and resonance frequencies are 0.7 GHz and 1.96 GHz with very low insertion and return losses, which make it appropriate for modern wireless applications. It has a wide FBW. The design steps are prepared as follows: First, a bandpass basic structure is presented and mathematically analyzed. The resonance frequency of this basic structure is achieved. Then, it upgraded to obtain a BPF. After that, a lowpass basic structure is proposed and analyzed mathematically. Next, it upgraded to obtain an LPF. Finally, the LPF and BPF are integrated to create our LP-BP diplexer. With a clear understanding of the operating frequency equation, designers can efficiently tune and fine-tune the diplexer's performance without the need for extensive simulations or prototyping. This can save time and resources during the design process.

# II. DESIGN STEPS

In Fig. 1, the basic bandpass structure used in this paper is shown. It includes a pair of microstrip coupled lines. The microstrip coupled lines are connected to a microstrip stub loaded thin meandrous line. Two solid cells are packed inside the meandrous line, which has capacitive features. These capacitors are effective in improving the frequency response. However, the most crucial cell in creating the passband is the microstrip coupled lines. Because they create some small capacitors, whereas the thin lines have an inductive feature. In Fig. 2, the equivalent LC model of this basic structure is depicted. The solid cells 1 and 2 are substituted by  $C_i$  and C<sub>2</sub> capacitors. In this circuit, the effects of coupling are presented only by a capacitor of  $C_3$ , which is an approximated model. This approximated LC circuit is acceptable with a high accuracy for the frequencies <10 GHz. The microstrip physical thin lines  $l_1$ -  $l_3$  are substituted by  $L_1$ -  $L_3$  inductors.

To analyze the basic bandpass structure, its ABCD matrix  $(M_{_{\rm BP\text{-}S}})$  is expressed as:

$$\mathbf{M}_{\mathrm{BP-S}} = \begin{bmatrix} 1 & j\omega \mathbf{L}_{3} \\ 0 & 1 \end{bmatrix} \times \begin{bmatrix} 1 & 0 \\ \frac{1}{j\omega \mathbf{L}_{3} + \frac{1}{j\omega \mathbf{C}_{0}}} & 1 \end{bmatrix} \times \begin{bmatrix} 1 & \frac{1}{j\omega \mathbf{C}_{3}} \\ 0 & 1 \end{bmatrix} \times \begin{bmatrix} 1 & 0 \\ \mathbf{y}_{1} & 1 \end{bmatrix} \times \begin{bmatrix} 1 & j\omega \mathbf{L}_{3} \\ 0 & 1 \end{bmatrix}$$
(1)

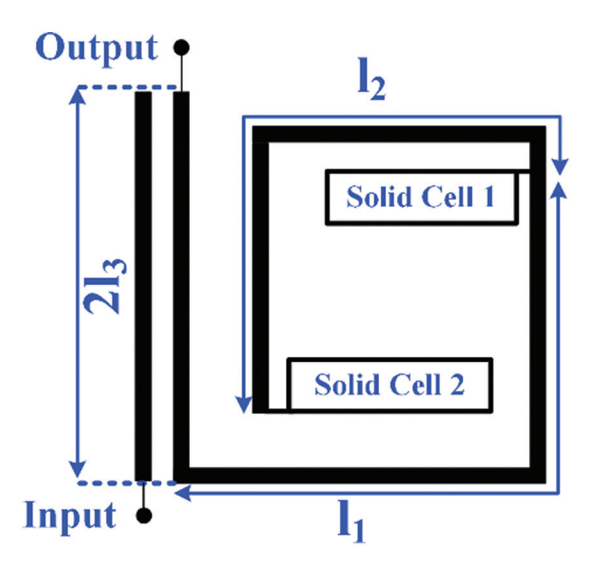


Fig. 1. Designed basic bandpass structure.

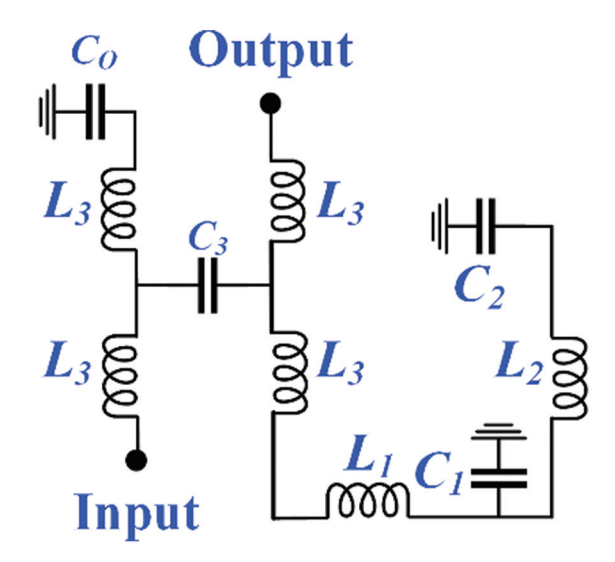


Fig. 2. LC model of the basic bandpass structure.

Since the open-end capacitor is tiny, it can be written that:

$$j\omega L_3 + \frac{1}{j\omega C_0} \approx \frac{1}{j\omega C_0}$$
 (2)

Also, the admittance  $y_i$  at the arbitrary angular frequency is calculated as follows:

$$y_{1} = \frac{1}{\left(\frac{1}{j\omega C_{2}} + j\omega L_{2}\right) \times \frac{1}{j\omega C_{1}}} + j\omega \left(L_{1} + L_{3}\right)$$

$$\frac{1}{j\omega C_{2}} + j\omega L_{2} + \frac{1}{j\omega C_{1}}$$
(3)

The range of coupling capacitor  $(C_1)$ , inductors  $(L_1, L_2, L_3)$ , and  $\omega$  are fF, nH, and GHz, respectively. Therefore, the following approximations are acceptable:

$$\frac{\left(\frac{1}{j\omega C_2} + j\omega L_2\right) \times \frac{1}{j\omega C_1}}{\frac{1}{j\omega C_2} + j\omega L_2 + \frac{1}{j\omega C_1}} \approx \frac{1}{j\omega C_2} + j\omega L_2$$
(4)

By placing equation (4) in (3), the following result is obtained:

$$y_1 \approx \frac{1}{\frac{1}{j\omega C_2} + j\omega (L_1 + L_2 + L_3)}$$
 (5)

After calculation, equation (1) will be obtained as follows:

$$M_{BP-S} = \begin{bmatrix} 1 - \omega^{2}C_{o}L_{3} + y_{1} \left(\frac{1 - \omega^{2}C_{o}L_{3}}{j\omega C_{3}} + j\omega L_{3}\right) \frac{1 - \omega^{2}C_{o}L_{3}}{j\omega C_{3}} \\ + j\omega L_{3} \left(2 - \omega^{2}C_{o}L_{3} + y_{1} \left(\frac{1 - \omega^{2}C_{o}L_{3}}{j\omega C_{3}} + j\omega L_{3}\right)\right) j\omega C_{o} + \\ y_{1} \left(1 + \frac{C_{o}}{C_{3}}\right) 1 + \frac{C_{o}}{C_{3}} + j\omega L_{3} \left(j\omega C_{o} + y_{1} \left(1 + \frac{C_{o}}{C_{3}}\right)\right) \end{bmatrix}$$
(6)

As mentioned before, the open-end capacitor is small so that:

$$C_0 C_3 \to 1 + \frac{C_0}{C_2} \approx 1 (7)$$

$$j\omega C_0 + y_1 \left( 1 + \frac{C_0}{C_3} \right) \approx y_1 \tag{8}$$

$$1-\omega^2 \, C \, 0 \, L \, 3 \approx 1$$
 (9)

After applying the approximations of equations (7), (8), and (9), the matrix  $M_{\text{RP-S}}$  will be simplified as follows:

$$\mathbf{M}_{\mathrm{BP-R}} \approx \begin{bmatrix} 1 + \frac{y_1}{j\omega C_3} + j\omega L_3 y_1 \frac{1}{j\omega C_3} + 2j\omega L_3 + \frac{y_1 L_3}{C_3} - \omega^2 L_3^2 y_1 \\ y_1 1 + j\omega L_3 y_1 \end{bmatrix} \tag{10}$$

If we connect the I/O ports to two microstrip cells with  $50\Omega$  impedances, the transmission parameter  $S_{21}$  will be extracted from equation (10) as follows [20]:

$$S_{21} = \frac{2}{\left(1 + \frac{y_1}{j\omega C_3} + j\omega L_3 y_1\right) + 0.02}$$
$$\left(\frac{1}{j\omega C_3} + 2j\omega L_3 + \frac{y_1 L_3}{C_3} - \omega^2 L_3^2 y_1\right) + 50y_1 + \left(1 + j\omega L_3 y_1\right)$$
(11)

Considering the small coefficient of 0.02, the following approximations can be applied in equation (11) with a high accuracy:

$$2 + \frac{0.02}{j\omega C_3} + 0.04j\omega L_3 \qquad 2 \tag{12}$$

$$50y_1 + \frac{y_1}{j\omega C_3} + 2j\omega L_3 y_1 \qquad 0.02 \frac{y_1 L_3}{C_3} - 0.02\omega^2 L_3^2 y_1 \tag{13}$$

By inserting equations (12) and (13) into equation (11), the following result will be obtained:

$$S_{21} \approx \frac{2}{2 + y_1 \left(\frac{1}{j\omega C_3} + 2j\omega L_3 + 50\right)}$$
 (14)

The resonance frequency is where the size of  $S_{2l}$  becomes one. Therefore, the resonance angular frequency  $(\omega_R)$  of the basic structure is expressed as follows:

$$\frac{1}{j\omega_{R}C_{3}} + 2j\omega_{R}L_{3} + 50 = 0 \rightarrow 1 - 2\omega_{R}^{2}C_{3}L_{3} + 50j\omega_{R}C_{3} = 0$$

$$= \begin{cases}
1 - 2\omega_{R}^{2}C_{3}L_{3} = 0 \rightarrow \omega_{R} = \sqrt{\frac{1}{2C_{3}L_{3}}} \\
&\text{and} \\
&\omega_{R}C_{3} \approx 0
\end{cases}$$
(15)

Equation (15) is not acceptable for the large values of C<sub>3</sub>, because the term  $\omega_R C_3$  cannot be near zero. As mentioned before C<sub>3</sub> is very small in fF. Therefore, equation (15) is acceptable where  $\omega_R$  is in GHz. Based on equation (15), we can tune the resonance frequency by adjusting  $L_3$ . Consequently, we can set  $\omega_R$  at a desired location by tuning the physical length l<sub>3</sub>. This verifies the importance of coupled lines. In fact, the passband will be generated by the coupled lines along with some microstrip cells to improve the frequency response. Using this basic structure, our resonator is designed and shown in Fig. 3. The input and output ports have  $50\Omega$  impedances. This structure is simulated using ADS software. It was simulated on a substrate with the  $\varepsilon$ =9.6 and h=25mil. This substrate has been used in other design stages for simulation as well as in the construction of the final device. The simulated frequency response of this resonator is illustrated in Fig. 4.

To improve the frequency response, another step impedance cell is added to the bandpass resonator. This structure is a BPF. In Figs. 5 and 6, the BPF layout and its frequency response are shown. This filter has 1.191 GHz center frequency, where the return and ILs are 22.297 dB and 0.028 dB. Its -3 dB cutoff frequencies are 1.66 GHz and 2.16 GHz. Therefore, it has a wide FBW% of 26.4%. Its GD is presented in Fig. 7. As shown, this filter has a flat GD lower than 1.2 ns from DC up to 3 GHz.

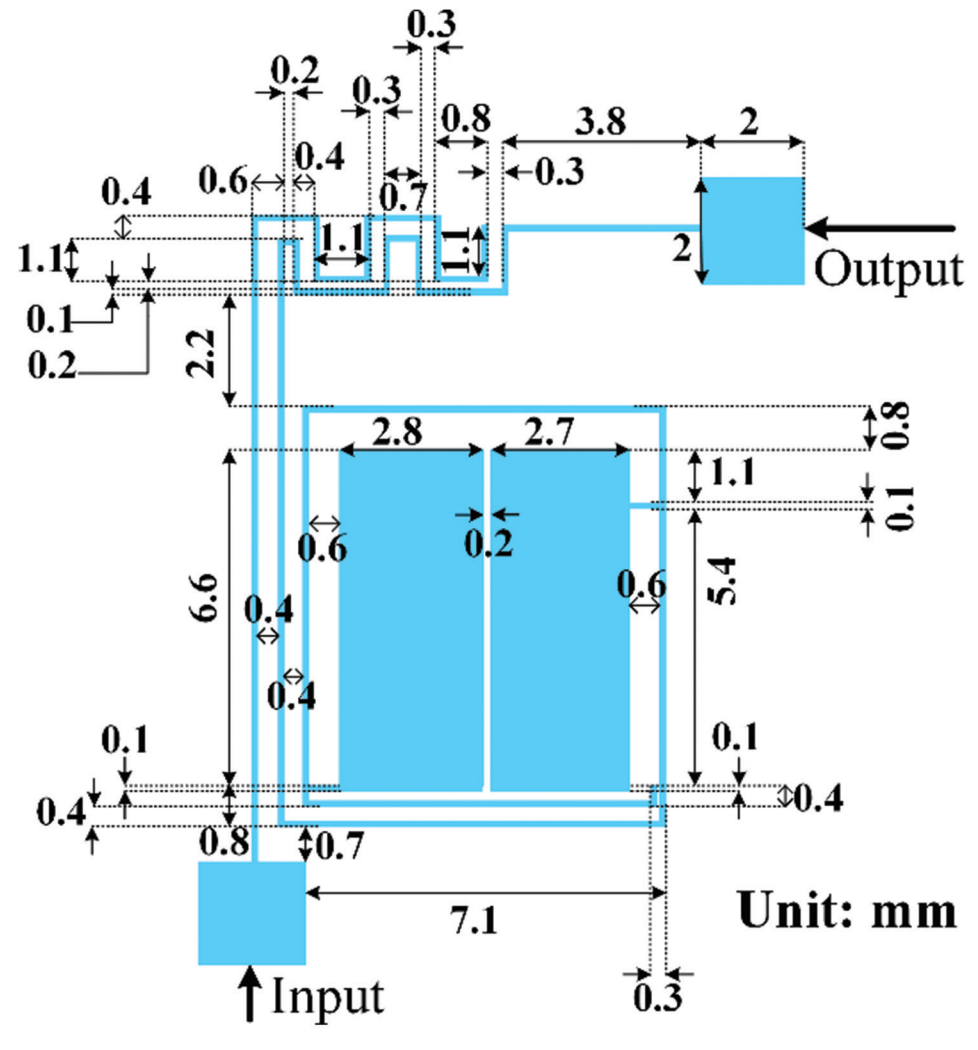


Fig. 3. Bandpass resonator.

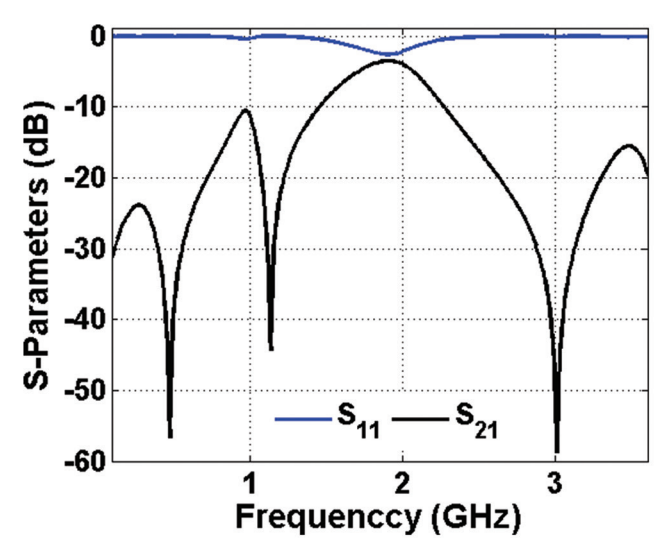


Fig. 4. Frequency response of the bandpass resonator.

The proposed basic lowpass structure includes a long microstrip meandrous thin line along with two shunt stubs. The stubs consist of thin lines connected to microstrip solid cells. The basic lowpass structure is shown in Fig. 8. Its approximated LC model is presented in Fig. 9, in which

we ignored the effects of steps. The solid cells 3 and 4 are replaced by the capacitors  $C_a$  and  $C_b$ . Moreover, the inductors  $L_4$ - $L_8$  are the equivalents of physical thin lengths  $l_4$ - $l_8$ .

Similar to the basic bandpass structure, for analyzing the basic lowpass structure, we can calculate its ABCD matrix as follows:

$$M_{LP-S} = \begin{bmatrix} 1 & j\omega L_8 \\ 0 & 1 \end{bmatrix} \times \begin{bmatrix} 1 & 0 \\ \frac{1}{j\omega L_6 + \frac{1}{j\omega C_a}} & 1 \end{bmatrix} \times \begin{bmatrix} 1 & j\omega L_6 \\ 0 & 1 \end{bmatrix} \times \begin{bmatrix} 1 & j\omega L_6 \\ 0 & 1 \end{bmatrix} \times \begin{bmatrix} 1 & j\omega L_6 \\ \frac{1}{j\omega L_5 + \frac{1}{j\omega C_b}} & 1 \end{bmatrix} \times \begin{bmatrix} 1 & j\omega L_4 \\ 0 & 1 \end{bmatrix}$$

$$(16)$$

Where:

$$A = \left(1 + \frac{j\omega L_8}{j\omega L_6 + \frac{1}{j\omega C_a}}\right) \left(1 + \frac{j\omega L_6}{j\omega L_5 + \frac{1}{j\omega C_b}}\right) + \frac{j\omega L_8}{j\omega L_5 + \frac{1}{j\omega C_b}}$$

$$(17)$$

ARO p-ISSN: 2410-9355, e-ISSN: 2307-549X

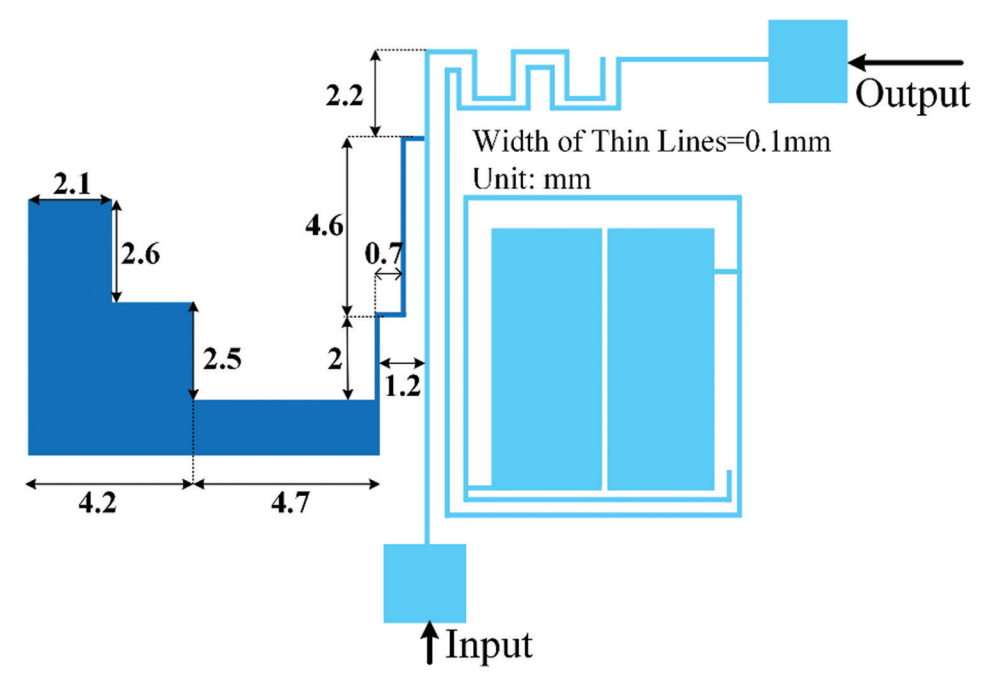


Fig. 5. Layout configuration of the proposed bandpass filter.

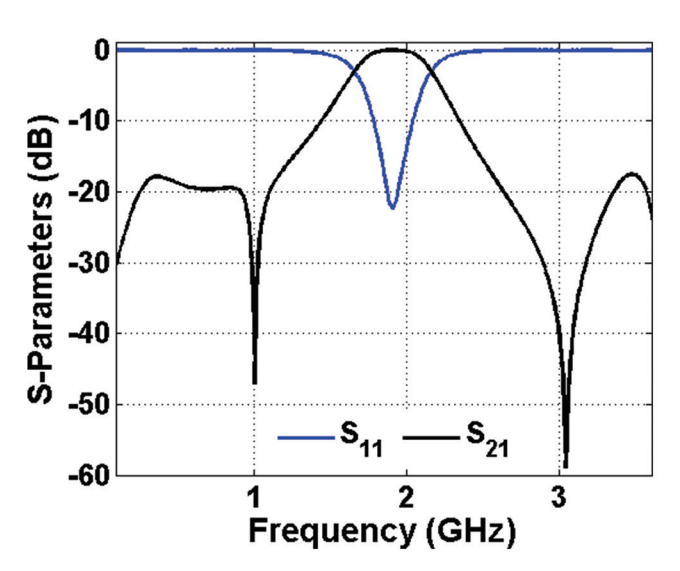


Fig. 6. The bandpass filter frequency response.

$$B = j\omega(L_8 + L_6) - \frac{\omega^2 L_8 L_6}{j\omega L_6 + \frac{1}{j\omega C_a}} + j\omega L_4$$

$$\left[ \left( 1 + \frac{j\omega L_8}{j\omega_6 + \frac{1}{j\omega C_a}} \right) \left( 1 + \frac{j\omega L_6}{j\omega L_5 + \frac{1}{j\omega C_b}} \right) + \frac{j\omega L_8}{j\omega L_5 + \frac{1}{j\omega C_b}} \right]$$

$$(18)$$

$$C = \left(\frac{1}{j\omega L_6 + \frac{1}{j\omega C_a}}\right) \left(1 + \frac{j\omega L_6}{j\omega L_5 + \frac{1}{j\omega C_b}}\right) + \frac{1}{j\omega L_5 + \frac{1}{j\omega C_b}}$$
(19)

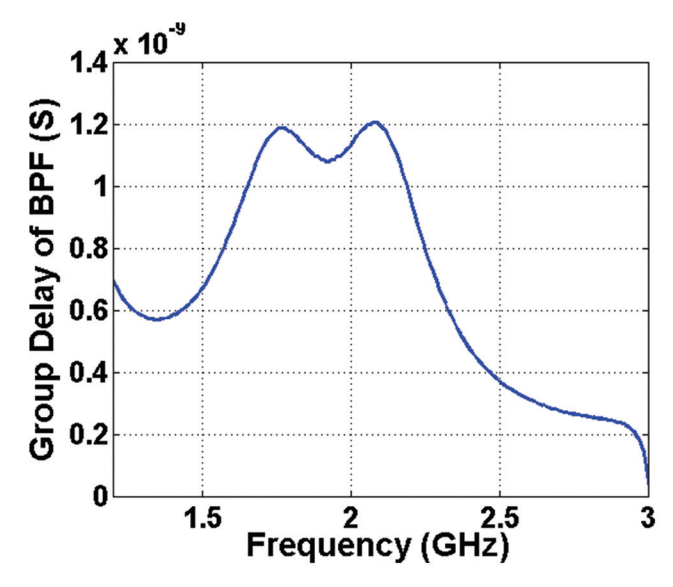


Fig. 7. The bandpass filter group delay.

$$= j\omega(L_8 + L_6) - \frac{1}{j\omega L_6} + \frac{1}{j\omega C_a} + j\omega L_4$$

$$D = 1 + \frac{j\omega L_6}{j\omega L_6 + \frac{1}{j\omega C_a}} + j\omega L_4$$

$$\left[ \left( 1 + \frac{j\omega L_8}{j\omega L_5 + \frac{1}{j\omega C_b}} \right) \left( 1 + \frac{j\omega L_6}{j\omega L_5 + \frac{1}{j\omega C_b}} \right) + \frac{j\omega L_8}{j\omega L_5 + \frac{1}{j\omega C_b}} \right] - \left[ \left( \frac{1}{j\omega L_6 + \frac{1}{j\omega C_a}} \right) \left( 1 + \frac{j\omega L_6}{j\omega L_5 + \frac{1}{j\omega C_b}} \right) + \frac{1}{j\omega L_5} + \frac{1}{j\omega C_b} \right]$$

$$(20)$$

The lowpass structure -3dB cutoff frequency is located, where  $|S_{21}|=|S_{11}|=3$  dB. Therefore, at  $\omega_c$ , where the impedances of terminals are  $50\Omega$ , we can write (Hong and Lancaster, 2001):

$$|S_{21}| = |S_{11}| = 3dB \rightarrow \left| \frac{2}{A + 0.02B + 50C + D} \right|$$

$$= \left| \frac{A + 0.02B - 50C - D}{A + 0.02B + 50C + D} \right| = 3dB$$
(21)

Hence:

$$A + 0.02B - 50C - D = 2 \tag{22}$$

Since the term 0.02B is significantly smaller than other terms, we can ignore it in equation (22). Furthermore, the term 50C is higher than the others. Hence, replacing equations (17), (18), (19), and (20) in equation (22) results:

$$\left| \frac{1}{j\omega_C L_6 + \frac{1}{j\omega_C C_a}} \right| \left( 1 + \frac{j\omega_C L_6}{j\omega_C L_5 + \frac{1}{j\omega_C C_b}} \right) + \frac{1}{j\omega_C L_5 + \frac{1}{j\omega_C C_b}} \right| = 0.04$$

$$\Rightarrow \left| \omega_C \left[ \frac{C_a}{1 - \omega_C^2 L_6 C_a} - \frac{\omega_C^2 C_b C_a L_6}{1 - \omega_C^2 L_5 C_b} \times \frac{1}{1 - \omega_C^2 L_6 C_a} + \frac{C_b}{1 - \omega_C^2 L_5 C_b} \right] = 0.04$$
 (23)

Since the left side of the last equation is a small real number close to zero, it is sufficient that the following relationship holds:

$$\frac{C_a}{1 - \omega_C^2 L_6 C_a} - \frac{\omega_C^2 C_b C_a L_6}{1 - \omega_C^2 L_5 C_b} \times \frac{1}{1 - \omega_C^2 L_6 C_a} + \frac{C_b}{1 - \omega_C^2 L_5 C_b} \approx 0 \quad (24)$$

Based on equation (24), the lowpass structure -3 dB cutoff frequency is:

$$\omega_C \approx \sqrt{\frac{C_a + C_b}{C_a C_b (L_5 + 2L_6)}} \tag{25}$$

Therefore, by increasing  $l_5$  and  $l_6$ , the cutoff frequency can move to the left. However, according to equation (25), the effect of increasing  $l_6$  is more than  $l_5$ . On the other hand, changing the dimensions of solid cells a and b can change the cutoff frequency in accordance with equation (25). Using the analyzed structure, a LPF is designed, as shown in Fig. 10. The simulation result of this structure is presented in Fig. 11. Its cutoff frequency is 730 MHz, with 0.041 dB low insertion loss, where the return loss is 20 dB.  $S_{21}$  is -20.9 dB at 1.17 GHz. Accordingly, this LPF has a roll-off of  $\xi = 38.6$  dB/GHz. The suppressed maximum level of harmonics is -17.68 dB at 2.6 GHz. Therefore, its RSB

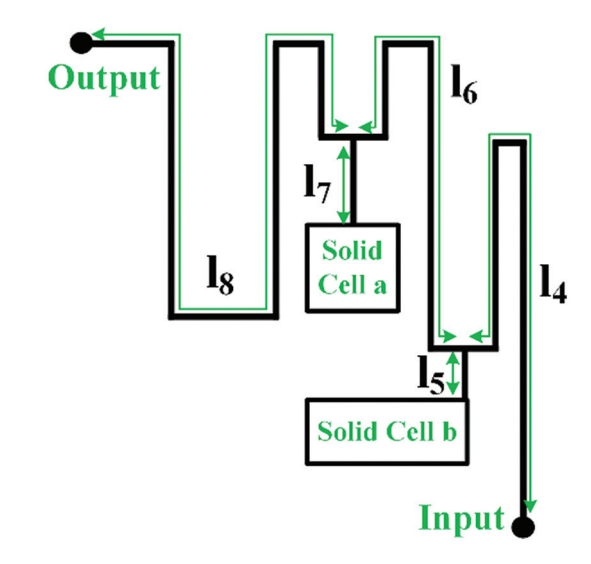


Fig. 8. Basic semi-layout structure of the designed lowpass structure.

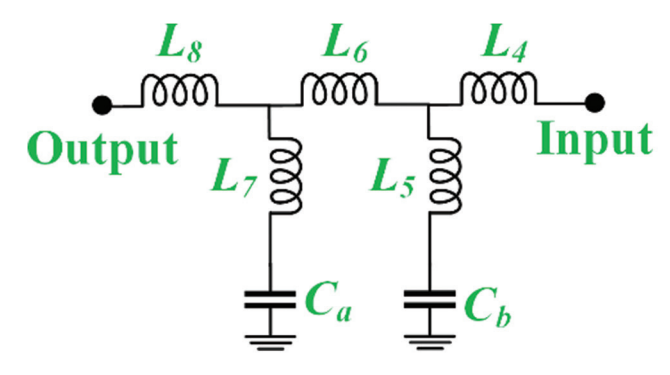


Fig. 9. The lowpass structure LC circuit.

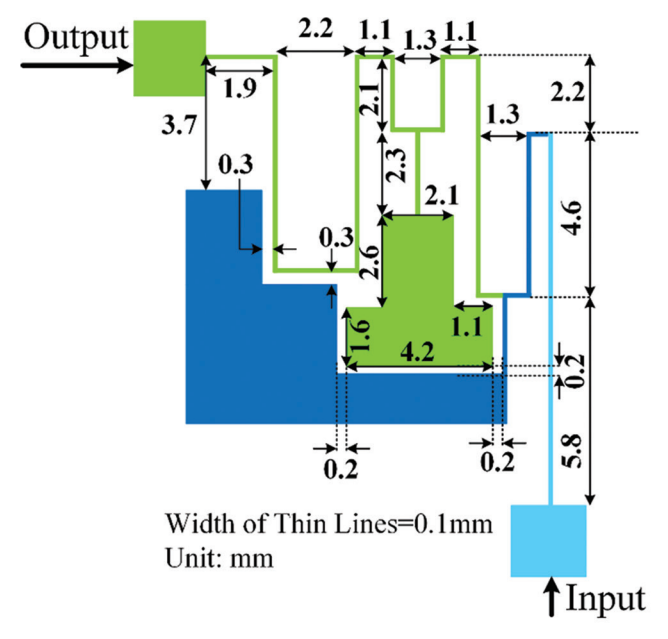


Fig. 10. The lowpass filter Layout.

(relative stopband bandwidth) and SF (suppression factor) are 2.56 and 1.768, respectively (Majidifar, 2016).

By connecting the designed LPF and BPF directly, we can obtain a LP-BP diplexer, as illustrated in Fig. 12.

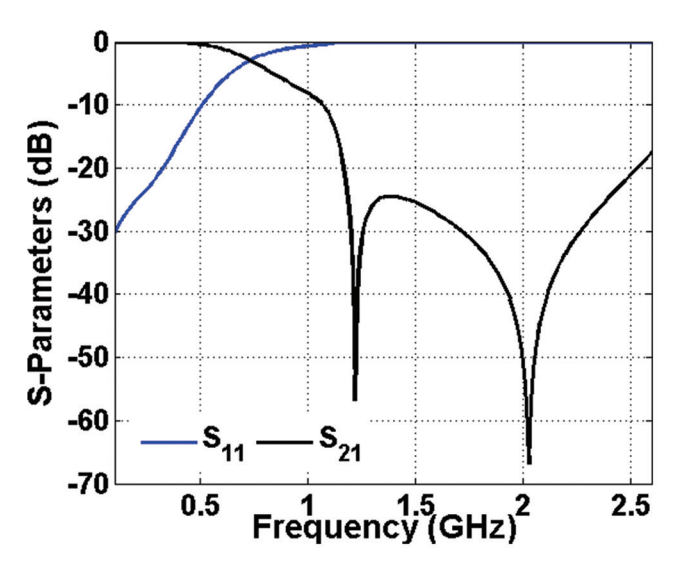


Fig. 11. The lowpass filter frequency response.

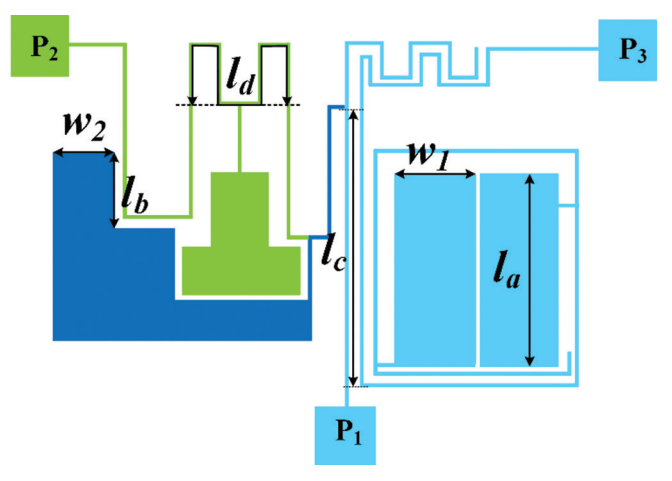


Fig. 12. Geometrical structure of the presented LP-BP diplexer.

The proposed diplexer size, including input/output, is 22.4 mm  $\times$  15.5 mm (0.12  $\lambda g \times 0.08 \lambda g$ ). All dimensions of this diplexer are exactly equal to the layouts presented in Figs. 3, 5, and 10. The final dimensions are optimized, as presented in Fig. 13. It can be seen that decreasing the length l<sub>2</sub> can destroy the bandpass channel. l<sub>3</sub> can change the cutoff frequency of the lowpass channel, which verifies equation (25). This length has an impact on the capacity of C<sub>b</sub>. The coupled lines physical length (l<sub>c</sub>) has an important effect on shifting the resonance frequency of bandpass channel. This fact is verified in equation (15). Furthermore, the optimization method and equation (15) confirm that by increasing the coupled lines length, the resonance frequency can move to the left. Meanwhile, the harmonics can be suppressed by tuning I<sub>d</sub>. Furthermore, by changing w<sub>1</sub> and  $w_2$ , we can control the harmonics of  $S_{31}$  and  $S_{21}$ , respectively. Since changing, can change the value of C<sub>b</sub>, it can shift the cutoff frequency, which is verified by equation (25). Hence, the optimization steps are verified by equations

(15) and (25). This means that, using the mathematical design method, the optimization is easier and faster.

### III. RESULTS AND COMPARISON

All simulation results are obtained using ADS software. Fig. 14 shows the simulated scattering parameters of our LP-BP diplexer. The simulated isolation between channels is depicted in Fig. 15. As presented in Fig. 14, the lowpass band is from DC up to 710 MHz (-3dB cut-off frequency).  $S_{21}$  reaches to -20 dB at 1.16 GHz, so that it has a roll-off of  $\xi = 37.78$  dB/GHz. The RSB, AF, and SF of lowpass section are 1.31, 1, and 1.9 (Majidifar, S., 2016). Therefore, it has a FOM higher than 23551, which is good for a LP-BP diplexer. The return and ILs at the first channel are 0.058 dB and 34.2 dB. Hence, The OFOM of lowpass section is higher than 13887.

The bandpass channel has two -3dB cutoff frequencies at 1.675 GHz and 2.18 GHz. Therefore, its FBW is 26.4%. The maximum harmonic value is -19.2 dB up to 3.35 GHz (4.7 F<sub>c</sub>). Furthermore, for -15 dB maximum harmonic level, the harmonics are suppressed from  $1^{st}$  up to  $4^{th}$  (5.07 F<sub>c</sub>). The second channel resonance frequency is  $F_R=1.95$  GHz, which makes it appropriate for mid-band 5G. In this channel, the insertion is 0.013 dB and the obtained return losses are 26.5 dB. Due to having connectors and copper losses, the isolation factor is better than -21.7 dB (Fig. 15). To demonstrate the superiority of this diplexer, we compared it with the previous LP-BP diplexers, as shown in Table I. As can be seen, compared to the smallest LP-BP diplexer (with a size of 0.03  $\lambda g^2$ ), the dimensions of our device are reduced by 33% (reduced to 0.01  $\lambda g^2$ ). Hence, our diplexer is the smallest LP-BP diplexer. In comparison with previous works, the losses of this diplexer are very low, whereas it has the widest FBW. Furthermore, the lowest insertion loss at 2<sup>nd</sup> channel is obtained in this work. Only the proposed LP-BP diplexers in Hayati, et al., 2021, and Heshmati and Roshani, 2018, could suppress the harmonics better than us. However, they have higher losses, larger sizes, and narrower bandpass channels than our diplexers. The overall comparison results show excellent performance with the smallest possible size.

The GD is an significant parameter in passive microstrip filtering devices because it affects the overall performance of the filter. GD is directly related to the time, it takes for different frequency components of a signal to transmit through a filter. If GD varies significantly with frequency, it can cause distortion in the output signal, leading to a degradation in signal quality. Moreover, it is closely related to phase linearity, which is crucial in maintaining the integrity of the signal waveform. A constant GD ensures that all frequency components of the input signal are delayed by the same amount, preserving the phase relationship between them. The GDs of S<sub>21</sub> and S<sub>31</sub> are illustrated in Figs. 16 and 17, respectively. In addition to the other advantages, our diplexer has low GD. In spite of the importance of GD factor, unfortunately, many previous microstrip designers have

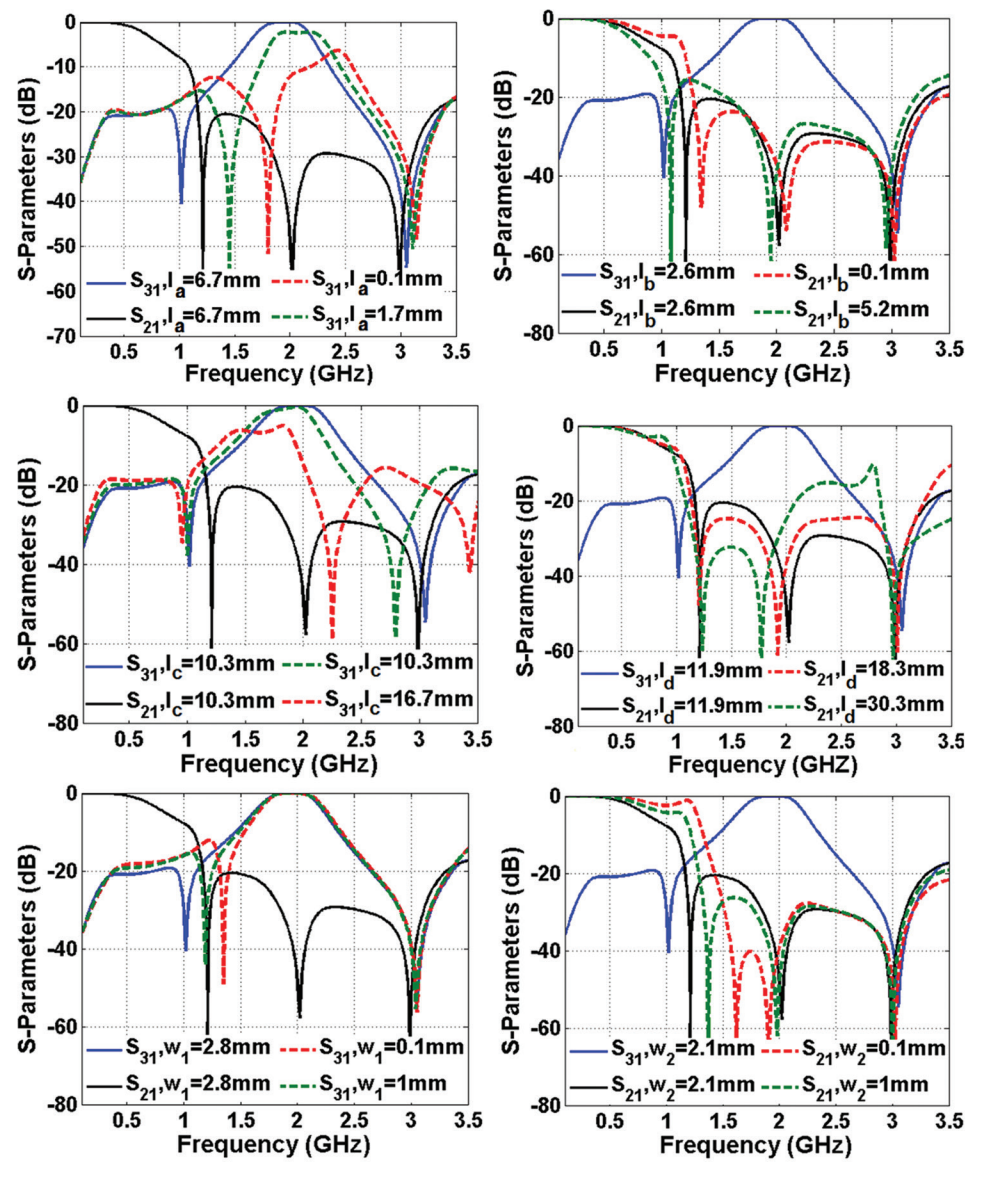


Fig. 13. A summary of the optimization steps.

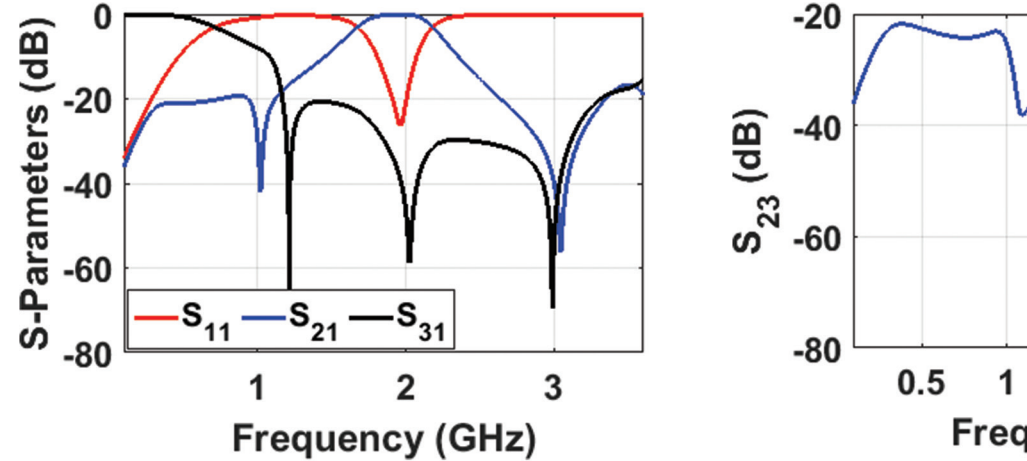


Fig. 14. The LP-BP diplexer frequency response.

not evaluated it. Thus, we had to compare the GD of our designed diplexer with some microstrip filtering designs in

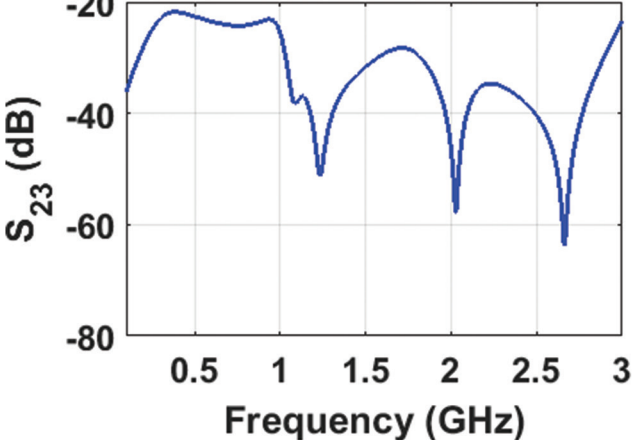


Fig. 15. Isolation between channels.

Table II. It can be seen that the best GD inside upper channel is belong to this diplexer.

 ${\rm TABLE}\; I$  Size and Performance Comparison, where All References are LP-bp Diplexers

References	$F_{C}, F_{R}$ (GHz)	$IL_1, IL_2(dB)$	RL <sub>1</sub> , RL <sub>2</sub> (dB)	Δ%	Upper stopband rejection	Size ( $\lambda g^2$ )
This work	0.71, 1.95	0.058, 0.013	34.2, 26.5	26.4	4.7 F <sub>C</sub>	0.01
(Rezaei, Noori and Jamaluddin, 2019)	2.4, 4.2	0.15, 0.1	18.2, 41.4	15.2	$3.2  \mathrm{F}_{\mathrm{C}}$	0.036
(Srikanth and Jeyalakshmi, 2014)	1.5, 2.4	0.1, 3.2		4.5	2.6 F <sub>C</sub>	
(Rayatzadeha and Moloudian, 2019)	1, 2.4	0.2, 0.8	10, 20	3.75	≈4.5 F <sub>C</sub>	
(Bavandpour, et al., 2021)*	2.3, 3, 6.2	0.2, 0.8, 1.2	Better than 20		2.8 F <sub>C</sub>	0.091
(Hayati, et al., 2021)	1.46, 2.42	0.68, 0.95	10.2, 16.8	11.13	5.1 F <sub>C</sub>	0.037
(Elden and Gorur, 2021)	2, 3.5	0.3, 1.2	15, 15	5.4	3 F <sub>C</sub>	0.095
(Deng and Tsai, 2013)	1.5, 2.4	0.25, 2.42		7.6	4 F <sub>C</sub>	
(Hayati, Rezaei and Noori, 2019)	1.88,3.56	0.12, 0.1	19.2, 36	23.8	4.45 F <sub>C</sub>	0.03
(Heshmati and Roshani, 2018)	1, 2.4	0.25, 0.5	15, 30		5 F <sub>C</sub>	0.046
(Nouri, Yahya and Rezaei, 2020)	2.64, 3.73	0.2, 0.2	18, 15.58	18.5	3.05 F <sub>C</sub>	0.075
(Perez, et al., 2019)	1.1, 2.4	0.15, 1.2	Better than 15	5	$3.3 F_{\rm c}$	
(Yahya, et al., 2020)	1.57, 3.35	0.01, 0.2	31, 16	4.7	2.8 F <sub>C</sub>	0.018
(Capstick, 1999)	1.5, 2.4	0.25, 2.4	15, 15		2 F <sub>C</sub>	0.49
(Rezaei, Yahya and Nouri, 2023)	1.65, 2.57	0.047, 0.1	21.8, 20.9	14	$2.4  \mathrm{F_c}$	0.03

(RL: Return loss; IL: Insertion loss; \*: Tri-channel LP-BP diplexer; δ: Fractional bandwidth)

 $TABLE \ II \\ A \ Comparison \ of \ Maximum \ Group \ Delays \ (GDs) \ Inside \ the \ Passbands$ 

References	Maximum GDs at each channel (ns)	Туре
This work	0.81, 1.24	Diplexer (LP-BP)
(Noori and Rezaei, 2017)	2.76, 3.31, 0.91, 2.15	Diplexer (Quad-Channel BP)
(Lin, 2011)	9, 6, 6, 5	BPF (Quad-Channel)
(Nouri, Yahya and Rezaei, 2020)	1.43, 1.68	Diplexer (LP-BP)
(Rezaei, et al., 2019)	2.6 for both channels	Diplexer (BP-BP)
(Majdi and Mezaal, 2023)	Near 4 *, near 3 *	Diplexer (BP-BP)
(Liu, Dou and Zhao 2010)	Better than 8 at all channels	BPF (Tri-Channel)
(Chen, et al., 2015)	1.5, 6, 4.4	Triplexer (LP-BP)
(Nouri, Yahya and Rezaei, 2020)	2.75, 2.25	Diplexer (BP-BP)
(Xu, Chen, Z.Y., and Wan, 2020)	1.62, 1.75, 2.07	Triplexer (LP-BP)
(Hayati, et al., 2021)	0.65 *, more than 2.5 *	Diplexer (LP-BP)
(Hayati, Rezaei and Noori, 2019)	2, 1.24	Diplexer (LP-BP)

(\*: Approx.). BPF: Band-pass filter

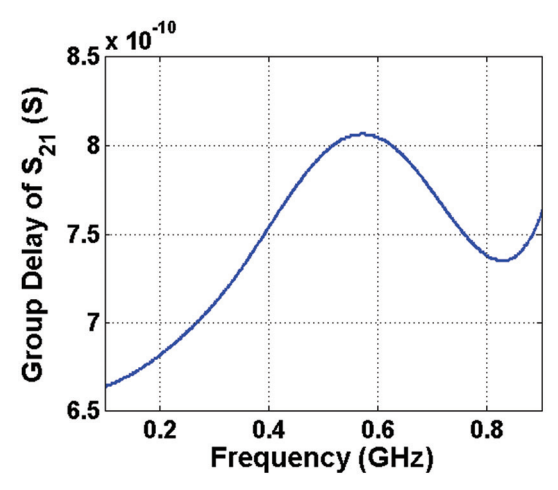


Fig. 16. Group delay of  $S_{21}$  inside the -3dB lowpass channel.

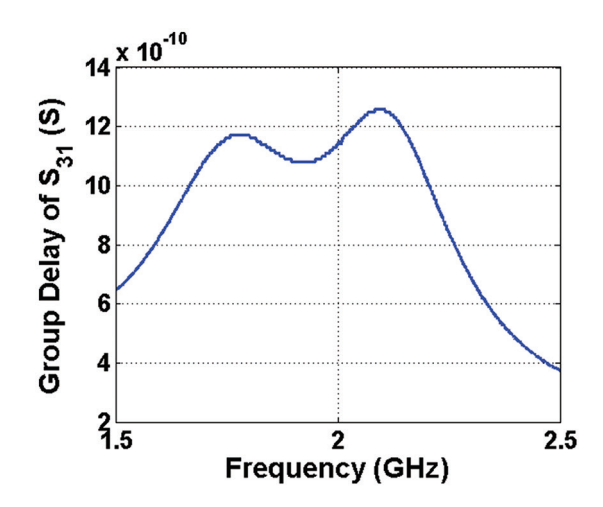


Fig. 17. Group delay of  $S_{31}$  inside the -3dB bandpass channel.

### IV. CONCLUSION

Our LP-BP diplexer with a novel microstrip structure, compact size, wide bandwidth, flat GDs, and operating frequencies at 0.71 GHz and 1.91 GHz presents a promising solution for various RF and microwave applications. The design's unique features, such as a thin meandered line loaded by the solid stubs, which are connected to coupled lines, contribute to its exceptional performance. The verification of equations and simulation results underscore the reliability and effectiveness of this diplexer design. The diplexer's compact size, high efficiency, and low ILs make it appropriate for many applications in radars, wireless communication, satellite, and microwave sensing. The operating frequency equation provided a predictive tool that enables designers to anticipate the diplexer's behavior under different conditions or variations in parameters. This helps in ensuring the diplexer's performance remains within specifications across different operating scenarios.

### REFERENCES

Bavandpour, S.K., Roshani, S., Pirasteh, A., Roshani, S., and Seyedi, H., 2021. A compact lowpass-dual bandpass diplexer with high output ports isolation. *AEU International Journal of Electronics and Communications*, 135, p.153748.

Capstick, M.H., 1999. Microstrip lowpass-bandpass diplexer topology. *Electronics Letters*, 35(22), pp.1958-1960.

Chen, F.C., Qiu, J.M., Hu, H.T., Chu, Q.X., and Lancaster, M.J., 2015. Design of microstrip lowpass-bandpass triplexer with high isolation. *IEEE Microwave and Wireless Components Letters*, 25(12), pp.805-807.

Deng, P.H., and Tsai, J.T., 2013. Design of microstrip lowpass-bandpass diplexer. *IEEE Microwave and Wireless Components Letters*, 23(7), pp.332-334.

Elden, S., and Gorur, A.K., 2021. Design of a compact lowpass-bandpass diplexer with high isolation. *Progress in Electromagnetics Research Letters*, 97, pp.21-26.

Hayati, M., Rezaei, A., and Noori, L., 2019. Design of a high-performance lowpass-bandpass diplexer using a novel microstrip structure for GSM and WiMAX applications. *IET Circuits, Devices and Systems*, 13(3), pp.361-367.

Hayati, M., Zarghami, A.R., Zarghami, S., and Alirezaee, S., 2021. Designing a miniaturized microstrip lowpass-bandpass diplexer with wide stopband by examining the effects between filters. *AEU-International Journal of Electronics and Communications*, 139, p.153912.

Heshmati, H., and Roshani, S., 2018. A miniaturized lowpass bandpass diplexer with high isolation. *AEU - International Journal of Electronics and Communications*, 87, pp.87-94.

Hong, J.S., and Lancaster, M.J., 2001. *Microstrip Filters for RF/Microwave Applications*. John Wiley & Sons, United States.

Jamshidi, M., Yahya, S.I., Nouri, L., Dezaki, H.H., Rezaei, A., and Chaudhary, M.A., 2023. A high-efficiency diplexer for sustainable 5G-enabled IoT in metaverse transportation system and smart grids. *Symmetry*, 15(4), p.821.

Lin, S.C., 2011. Microstrip dual/quad-band filters with coupled lines and quasi-lumped impedance inverters based on parallel-path transmission. *IEEE Transactions on Microwave Theory and Techniques*, 59(8), pp.1937-1946.

Liu, Y., Dou, W.B., and Zhao, Y.J., 2010. A tri-band bandpass filter realized using tri-mode T-shape branches. *Progess in Electromagnetics Research*, 105, pp.425-444.

Majdi, K.A., and Mezaal, Y.S., 2022. Microstrip diplexer for recent wireless communities. *Periodicals of Engineering and Natural Sciences*, 10(1), pp.387-396.

Majdi, K.A., and Mezaal, Y.S., 2023. New miniature narrow band microstrip diplexer for recent wireless communications. *Electronics*, 12, p.716.

Majidifar, S., 2016. Design of high performance miniaturized lowpass filter using new approach of modeling. *ACES Journal*, 31(1), pp.52-57.

Noori, L., and Rezaei, A., 2017. Design of a microstrip diplexer with a novel structure for WiMAX and wireless applications. *AEU - International Journal of Electronics and Communications*, 77, pp.18-22.

Nouri, L., Yahya, S.I., and Rezaei, A., 2020. Design and fabrication of a low-loss microstrip lowpass-bandpass diplexer for WiMAX applications. *China Communications*, 17(6), pp.109-120.

Nouri, L., Yahya, S.I., Rezaei A., Hazzazi, F., and Nhu, B.N., 2023. A compact negative group delay microstrip diplexer with low losses for 5G applications: Design and analysis. *ARO-The Scientific Journal of Koya University*, 11(2), pp.17-24.

Perez, C., Yau, J.R.L., Hernandez, I.L., Moreno, P., Reynoso-Hernandez, A.J., and Lobo, L.M.A., 2019. Compact microstrip lowpass-bandpass diplexer using radial stubs. *Microwave and optical Technology Letters*, 61(2), pp.485-489.

Rayatzadeha, S., and Moloudian, G., 2019. Design and fabrication of a miniaturized lowpass-bandpass diplexer with wide tuning range and high isolation. *Journal of Electromagnetic Waves and Applications*, 33(14), pp.1874-1889.

Rezaei, A., Noori, L., and Jamaluddin, M.H., 2019. Novel microstrip lowpass-bandpass diplexer with low loss and compact size for wireless applications. *AEU-International Journal of Electronics and Communications*, 101, pp.152-159.

Rezaei, A., Yahya, S.I., and Nouri, L., 2023. Design and analysis of a compact microstrip lowpass-bandpass diplexer with good performance for wireless applications. *International Journal of Microwave and Wireless Technologies*, 15(7), pp.1099-1107.

Rezaei, A., Yahya, S.I., Noori, L., and Jamaluddin, M.H., 2019. Design of a novel wideband microstrip diplexer using artificial neural network. *Analog Integrated Circuits and Signal Processing*, 101, pp.57-66.

Roshani, S., Yahya, S.I., Ghadi, Y.Y., Roshani, S., Parandin, F., and Yaghouti, B.D., 2023. Size reduction and harmonics suppression in microwave power dividers: A comprehensive review. *ARO-The Scientific Journal of Koya University*, 11(2), pp.122-136.

Srikanth, S., and Jeyalakshmi, V., 2014. Design and implementation of microstrip lowpass-bandpass diplexer on FR-4 substrate. *International Journal of Advanced Research in Electrical, Electronics and Instrumentation Engineering*, 3(3), pp.355-359.

Taghvaei, A., Bayderkhani, R., and Espahbodi, M., 2022. Design and fabrication of adjustable reflectionless microstrip diplexer for L-band. *Progress in Electromagnetics Research C*, 126, pp.173-181.

Xu, J., Chen, Z.Y., and Wan, H., 2020. Lowpass-bandpass triplexer integrated switch design using common lumped-element triple-resonance resonator technique. *IEEE Transactions on Industrial Electronics*, 67(1), pp.471-479.

Yahya, S.I., Rezaei, A., and Nouri, L., 2021. A novel miniaturized microstrip lowpass-bandpass diplexer using patch and interdigital cells for wireless networks. *AEU - International Journal of Electronics and Communications*, 126, p.153404.

Yahya, S.I., Zubir, F., Hafez, M.A., Nouri, L., Chaudhary, M.A., Assaad, M., Rezaei, A., and Jizat, N.M., 2025. Novel high-performance microstrip diplexer for 5G mid-band and wide-band applications: Design, analysis and manufacturing. *PLoS One*, 20(7), p.e0327839.